Optical and Quantum Electronics (2023) 55:700
https://doi.org/10.1007/s11082-023-04981-9

Poly(3-hexylthiophene) incorporated with metallic nanoparticles: optoelectronic properties in context of organic solar cell

Saqiba Riaz[1] · Muhammad Azhar Ansari[2] · Daim Asif Raja[2] · Hajira Tahir[1] · Muhammad Imran Malik[2]

Received: 28 February 2023 / Accepted: 19 May 2023 / Published online: 8 June 2023

Abstract
Solar cells are employed to convert solar energy into electrical energy. High-cost and inherent environmental issues associated with commercially available inorganic solar cell production demand development of new alternatives. An obvious alternative in this context is organic material-based solar cells owing to their low cost and simplicity of production. Although, organic solar cells have achieved high conversion efficiencies (greater than 18%), the low stability and limited lifetime have hampered their use on commercial scale. Improvement in the optoelectronic properties of donor and acceptor materials is the primary method for improvement in its efficiency. Herein, we report incorporation of different metallic nanoparticles (MNPs) such as silver (Ag), gold (Au), cobalt (Co), copper (Cu), iron (Fe), and nickel (Ni) in poly(3-hexylthiophene), P3HT, the most widely used donor material, and compared their optoelectronic properties. The size and morphology of the synthesized P3HT-MNPs were determined by atomic force microscopy, scanning electron microscopy, and zatasizer while metal-polymer interactions were studied by FTIR spectroscopy. Finally, the effect of incorporation of different MNPs in P3HT on the optoelectronic properties was evaluated by UV–Vis spectrophotometry and cyclic voltammetry. A significant change in the optoelectronic properties by incorporation of different MNPs in P3HT opens possibilities of tuning the donor materials as per energy levels of acceptor material.

Keywords Poly(3-hexylthiophene) · P3HT · Metal nanoparticles · Energy band gap · HOMO–LUMO energy levels · Optoelectronic properties · Organic solar cell (OSC)

✉ Muhammad Imran Malik
mimran.malik@iccs.edu; m.imran.malik1@gmail.com

[1] Department of Chemistry, University of Karachi, Karachi 75270, Pakistan

[2] Third World Center for Science and Technology, H.E.J. Research Institute of Chemistry, International Center for Chemical and Biological Sciences (ICCBS), University of Karachi, Karachi 75270, Pakistan

1 Introduction

Affordable and clean energy is 7th while climate action is 13th sustainable development goal (SDG) out of 17 SDGs established by United Nations General Assembly in 2015. SDG-7 targets access to sustainable, reliable, economical, and modern energy for everyone. In this context, solar energy has the highest potential in comparison to other renewable energy sources (Franco et al. 2020). Photovoltaic (PV) device is a promising innovation that can be used to convert solar energy into electrical energy. Solar energy is a potent source of electricity with zero pollution rate; therefore, photovoltaic power generation has the ability to resolve the energy issues of the next generation. Solar cells are available in many designs and types, majorly inorganic solar cell and organic solar cell (OSC). Silicon-based inorganic solar cells that also contain gallium and cadmium, are energy-efficient and have captured the major share of the current market. Nevertheless, there are certain caveats associated with commercial inorganic solar cells for instance, manufacturing at high temperature and limited ability to integrate with other technologies such as building integrated photovoltaics (BIPV), greenhouse Integrated photovoltaics (GIPV), and automobiles. Hence, replacement of widely employed inorganic solar cell by eco-friendly alternatives is one of the targets of modern scientific research. OSCs can be an excellent alternative to overcome limitations of inorganic solar cell. However, OSC technology requires substantial improvement in terms of potency, environment, greener production, and cost adequacy (Mathews et al. 2019). Initially, OSC had very low power conversion efficiency (PCE) compared to crystalline Si-based inorganic photovoltaic cells (Chen et al. 1995). However, OSCs technology is improving rapidly in terms of PCE. Till date, the highest PCE of 19.2% for single junction OSC is reported by Zhu et al. (Zhu et al. 2022) that is high enough from commercialization perspective. However, the stability and lifetime of OSCs are still significantly low compared to Si-based solar cell (Xu et al. 2021). Nonetheless, the peculiar advantages associated with them are their light weight (Zhang et al. 2011; Zhou et al. 2011), ambient temperature and ambient pressure manufacturing (Perepichka and Bryce 2005; Eakins et al. 2011), and manufacturing in solution (Huang et al. 2012). An electron donor and an electron acceptor are the two major components constituting any OSC. Electron donor materials in this regard could be conjugated polymers such as poly(3-hexylthiophene) (P3HT), PTQ10, and PBDB-T-SF. On the other hand, fullerene, Y6, and ITIC are the widely employed electron acceptor materials (Ludwigs 2014; Sun et al. 2018; Zhao et al. 2017; Ameri et al. 2013; Yang 2021). The efficiency of OSC mainly depends upon the optoelectronic properties of these two materials (Gao et al. 2017). Low-cost, thermal stability, environment friendliness, and easy processability of polythiophenes (P3HT being the most prominent) makes them widely explored p-type donor materials for OSC (Cheng et al. 2009). However, commercial applications of P3HT as donor material in OSC are impeded by its high HOMO energy level and wide energy band gap (Liu et al. 2016). The intense part of solar radiations (red and infrared region) is not efficiently absorbed by P3HT owing to its large energy band gap. Enhancement in the absorption of the radiations from the solar spectrum can be realized by compression of HOMO–LUMO energy levels gap, which is possible by downshifting of LUMO or upshifting of HOMO energy levels (Gao et al. 2017; Peet et al. 2007; Leclerc et al. 2006; Kroon et al. 2008). Reduction in the energy band gap can also be achieved by increasing regioregularity and molar mass (Ballantyne et al. 2008b; Schilinsky et al. 2005; Trznadel et al. 1998; Ansari et al. 2018), and by p-doping (Jenkins et al. 2014; Ratcliff et al. 2010; Skompska and Szkurłat 2001). Moreover, molecular level modification in the chemistry of the parent donor and acceptor

materials may also facilitate the exciton movement (Perepichka and Bryce 2005; Huang et al. 2012; Brédas and Heeger 1994; Zhang et al. 2021; Ansari et al. 2022). However, the commercially feasible PCE and stability of OSC has not yet been achieved despite its huge potential (Li et al. 2022).

The light absorption of polymeric organic semiconductors is also impeded by its low charge carrier mobility (generally less than 10^{-4} cm^2/Vs) (Saeki et al. 2008) that restrict the thickness of the organic active layer to < 100 nm (Blakesley and Neher 2011; Gan et al. 2013). The incorporation of nanostructures in the OSC may facilitate the charge carrier mobility (Chen et al. 2019; Kango et al. 2013). Polymer nanowires provide percolation pathways for electrons and holes that ultimately improve the device efficiency (Xin et al. 2008; Xin et al. 2010). Stuart and Hall demonstrated up to 20-fold boost in the photocurrent by coating of AgNPs on the surface of a silicon-on-insulator (Stuart and Hall 1998). Metallic nanoparticles (MNPs) can disperse light and induce local surface plasmon resonance (SPR) between them. This phenomenon laid the foundation of many important commercial applications such as light-harvesting technologies, photocatalytic water splitting, photovoltaic, thermoelectric and photodynamic therapy platforms etc. (Boriskina et al. 2013; Zhou et al. 2015; Warren and Thimsen 2012). MNPs help in improvement of light absorption properties by serving as a 'light-trapping' agent in Organic photovoltaic (OPV) (Mbuyise et al. 2021), where the thickness of active layer has to be below 100 nm.

MNPs of different morphologies and sizes can induce surface plasmon effects in OPV applications. There can be three operative mechanisms based on their position in the OPV: (1) light scattering, (2) surface plasmon polaritons (SPP), and (3) localized surface plasmon resonance (LSPR). The incorporation of MNPs in organic active layer can improve the light absorption of the active layer owing to multiple light scattering by large sizes of MNPs or by excitation of LSPR modes by tiny sizes of MNPs (Sachchidanand and Samajdar 2019). The overlapping absorption bands of MNPs and conjugated polymers indicate the synergistic nature of their combination. The coherent oscillation of free electrons, which is exhibited as plasmon waves stimulated by the incident electromagnetic field, is the physical cause of the higher absorption of the composite. MNPs can function as centers for light scattering, enhancers of local field. MNPs may have dual function as scatterer and enhancer depending on their size. Absorption predominates for tiny MNPs having a diameter in a range of 5–20 nm. Due to the LSPR excitation in this scenario, the MNP behaves like a sub-wavelength antenna. On the contrary, MNPs having relatively large diameter (> 50 nm) operate as efficient sub-wavelength scatterers that render coupling and trapping of freely propagating plane waves of incident light into the photoactive layer (Zhang et al. 2019; Kravets et al. 2018). When photon energy excites the MNPs, the excited electrons that are dispersed in their outer orbitals are immediately transported to the active layer close to the MNPs (Yao et al. 2019). Hence, a careful design and optimization of MNPs is imperative to have a net beneficial impact on PCE of OSCs. In OSCs, conjugated polymers containing thiophene rings, such as poly(3-hexylthiophene) (P3HT), play important role as electron donors and in charge transportation (Padinger et al. 2003; Hoppe and Sariciftci 2004; Li et al. 2007). The incorporation of MNPs with polythiophene or P3HT may induce synergistic effect in their optoelectronic properties compared to the parent materials. For instance, composite of MNPs (such as aluminum, copper, and silver) with polythiophene is used for the humidity sensor owing to its high hole mobility, good stability, and better conductivity (Abdullah and Ibrahim 2021). Doping of plasmonic MNPs (for example, CuNPs) on the thin film of P3HT resulted in a 5–20 folds increase in its photoconductivity due to better charge separation process (Szeremeta et al. 2011). On the same lines, the absorption of AuNPs-P3HT composite shifted to longer wavelength (Bathochromic shift) compared to

the parent materials (Jana et al. 2015). Improvement in optical properties (such as photoluminescence) of P3HT by incorporation of AuNPs may be attributed to structural changes in the polymer film (Nicholson et al. 2005). P3HT can also serve as stabilizing agent for MNPs that ultimately lead to an increase in the strength of the material. The incorporation of MNPs in P3HT render a flexible, strong and efficient OSC (Kuila et al. 2007). Taking the motivation from the above-mentioned studies, P3HT capped MNPs using several metals such as silver (Ag), gold (Au), cobalt (Co), cupper (Cu), iron (Fe), and nickel (Ni) were prepared and analyzed in context of their characterization of nanostructure morphologies by atomic force microscopy (AFM), scanning electron microscopy (SEM), and dynamic light scattering (DLS). Finally, the optoelectronic properties of P3HT-MNPs are evaluated by UV–Vis spectrophotometry and Cyclic Voltammetry (CV). The comparative analysis of different MNPs incorporated with P3HT for optoelectronic properties is presented in the context of OSC.

2 Experimental section

2.1 Materials

Monomer 3-hexylthiophene was purchased from Ossila limited, UK. Toluene, tetrabutylammonium bromide (TBAB), tetrachloroauric (III) acid trihydrate ($HAuCl_4.3H_2O$) procured from Merck, Germany. Silver Nitrate ($AgNO_3$), nickel (II) chloride hexahydrate ($NiCl_2.6H_2O$), copper (II) Nitrate hydrate ($Cu(NO_3)_2.3H_2O$), cobalt (III) nitrate hexahydrate [$Co(NO_3)_3.6H_2O$], iron (III) chloride hexahydrate ($FeCl_3.6H_2O$), sodium borohydride ($NaBH_4$) were purchased from Sigma–Aldrich, Germany, and HPLC grade methanol from Tedia, USA. All the reagents were used as received.

2.2 Synthesis of P3HT

Synthesis of P3HT was conducted through oxidative coupling of 3-hexylthiophene (monomer) in the presence of ferric chloride ($FeCl_3$) as elaborated in detail in our recent publications (Ansari et al. 2018; Kaçuş et al. 2020). Briefly, a solution of $FeCl_3$ was made by dissolving its 3.86 g in 30 mL chloroform under nitrogen atmosphere in a 2-neck round bottom flask. After continuous stirring of almost 30 min, 1.0 mL of 3-hexylthiophene was added drop-wise followed by stirring for 24 h. The synthesized P3HT was then precipitated in methanol (app. 300 mL). The purification of P3HT was done in Soxhlet assembly by methanol. Finally precipitates of P3HT were dissolved in chloroform and dried again to get pure P3HT.

2.3 Preparation of P3HT incorporated MNPs

Metal nanoparticles of silver (Ag), gold (Au), cobalt (Co), cupper (Cu), iron (Fe), and nickel (Ni) were prepared by a two-phase (toluene/water) one-step method using P3HT as capping polymer. Briefly, the solutions of 0.01 mmol of respective metal salts ($AgNO_3$, $HAuCl_4.3H_2O$, $Co(NO_3)_3.6H_2O$, $Cu(NO_3)_2.3H_2O$, $FeCl_3.6H_2O$, and $NiCl_2.6H_2O$) were prepared in deionized (DI) water. In parallel, TBAB was dissolved in toluene, $NaBH_4$ was dissolved in DI water, and P3HT was dissolved in toluene. P3HT-MNPs were prepared as per reported procedure (Monnaie et al. 2013; Topp et al. 2010). 8.0 mL of TBAB solution

in toluene containing 0.05 mmol TBAB was mixed with 3.0 mL aqueous solution of metallic salts under vigorous stirring in round bottom flasks. TBAB acts as a phase changer here. When aqueous medium become transparent, the P3HT solution (1.5 mg P3HT dissolved in 3 mL toluene) was added under stirring. In this mixture, freshly prepared aqueous solution of $NaBH_4$ (10 mmol in 2.5 mL) was added drop-wise slowly within 2 h under stirring and the mixture was stirred overnight. Thereafter, the process was quenched by the addition of methanol in the mixture. The resulting mixture was filtered by PTFE membrane filter followed by washing with methanol and water to obtain P3HT-MNPs (de Freitas et al. 2012; Lu et al. 2013; Inagaki et al. 2018b). The final molar ratio of P3HT (8500 g/mol)-metal was 1.7/100.

2.4 Characterization

FT-IR spectroscopic analyses of P3HT and P3HT-MNPs were performed, by making KBr disks, in the spectral range of 4000–500 cm^{-1}. Nano-ZSP (Malvern Instruments) (zeta sizer) was used to determine the particle size and zeta potential. Topographical images of P3HT-MNPs in tapping mode were captured by atomic force microscope (Agilent 5500). One drop of the sample was placed on a silicon wafer that was freeze-dried for 24 h. For analysis of the sample, triangular nitride silicon cantilever (Veeco, model MLCT-AUHW) was used under a constant spring value of 0.1 Nm^{-1}. For SEM analysis, all P3HT-MNPs samples were mounted on electrically conductive, non-porous adhesive carbon tape. Images were recorded using a JEOL (Akishima, Tokyo, Japan), JSM-6380LV SEM microscope at an acceleration voltage of 10 kV.

UV–Visible-near IR Spectra of P3HT-MNPs films made from their toluene solutions were recorded in the wavelength range of 200–800 nm. P3HT-MNPs were coated on the quartz slide by drop casting method and spectra were recorded. The optical energy band gap (eV) is calculated from Wavelength Edge (λ_{edge}) of the absorbance peak using formula.

$$A = hC/\lambda$$

Where h is the Plank's constant having value 6.626×10^{-34} Joule second, C is the speed of light having value 3.0×10^{8} m/sec, and λ_{edge} is cut-off or onset wavelength. After calculating E in the unit of Joules from λ_{edge} (nm), it is converted into eV by dividing with 1.6×10^{-19}.

For cyclic voltametric studies, cell was equipped with working electrode of P3HT-MNPs coated ITO glass slide, a counter electrode of platinum, and a double junction reference electrode Ag/AgCl (0.1 M $AgNO_3$ in water). As supporting electrolyte, 0.1 M solution of tetrabutylammonium hexafluorophosphate ($TBAFP_6$) in acetonitrile was used. Cyclic voltammograms (CVs) were recorded after purging solution with nitrogen gas using a Potentiostat, CH Instrument, USA, Model CHI 660. Drop casting method was used to coat P3HT-MNPs on Indium tin Oxide (ITO) glass slide which were dried at ambient conditions. Finally, the CV were recorded by scanning at a rate of 100 mV/s from potential 0 to + 2 V, + 2 to 0, 0 to − 2, and finally from − 2 to 0.

3 Results and discussion

The most economical method for synthesis of P3HT is oxidative coupling of 3-hexylthiophene by using $FeCl_3$. Although this method has comparatively less control over molar mass and regioregularity, these can be improved significantly by choosing appropriate reaction conditions (Ansari et al. 2018, 2022). P3HT used in this study has a comparatively broad molar mass distribution (M_n: 8500 g/mol, Mw: 19,800 g/mol, Đ: 2.32) and has more than 70% HT sequences, see Fig. 1 in our recent publication (Ansari et al. 2022). Same sample of P3HT is used in this study throughout for a fair comparison of the optoelectronic properties of the subsequent nanocomposites of different metals such as silver, gold, cobalt, copper, iron and nickel.

3.1 Characterization of P3HT-MNPs

P3HT can be a good stabilizing agent for MNPs owing to presence of sulfur and thiophene ring (Inagaki et al. 2018b). MNPs incorporated with P3HT using different metals namely silver, gold, cobalt, copper, iron and nickel, but same P3HT sample were prepared and their topographical AFM images are depicted in Fig. 1. MNPs of the above-mentioned metals have fairly spherical morphology and are well-segregated from each other. However, the sizes of P3HT-MNPs for different metals are significantly different despite same procedure was used for their preparation (Shnoudeh et al. 2019). In order to further confirm the shape, morphology, and size of the prepared P3HT-MNPs, SEM images are depicted in Fig. 2. P3HT-MNPs of different metals have predominantly spherical shape but differ from each other in the size of particles, in some cases bimodality is also noticed. P3HT-AgNPs have similar size range of 100–150 nm along with fairly low number of particles having size approaching 200 nm. The size of P3HT-AuNPs is small compared to P3HT-AgNPs and most of the particles fall in range of 30–40 nm having fairly monomodal distribution. P3HT-CoNPs have most of the particles in a size range of 100–140 nm, however small

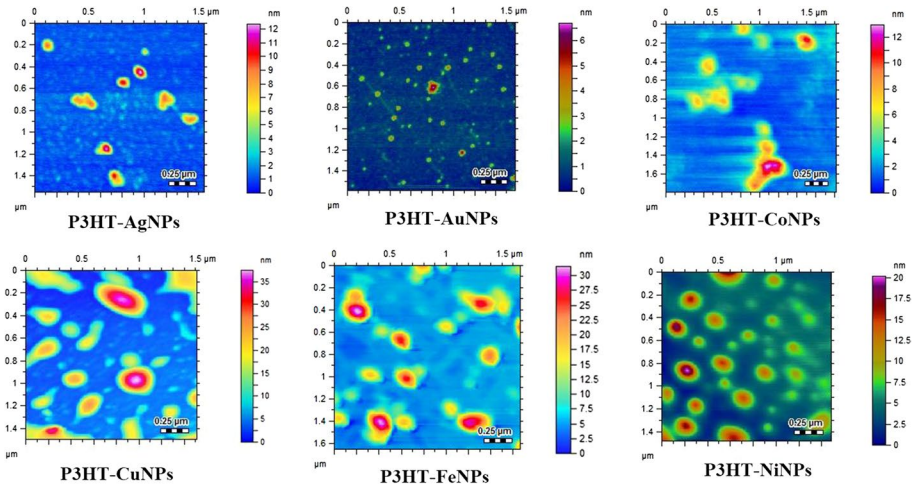

Fig. 1 AFM topographical images of P3HT-MNPs

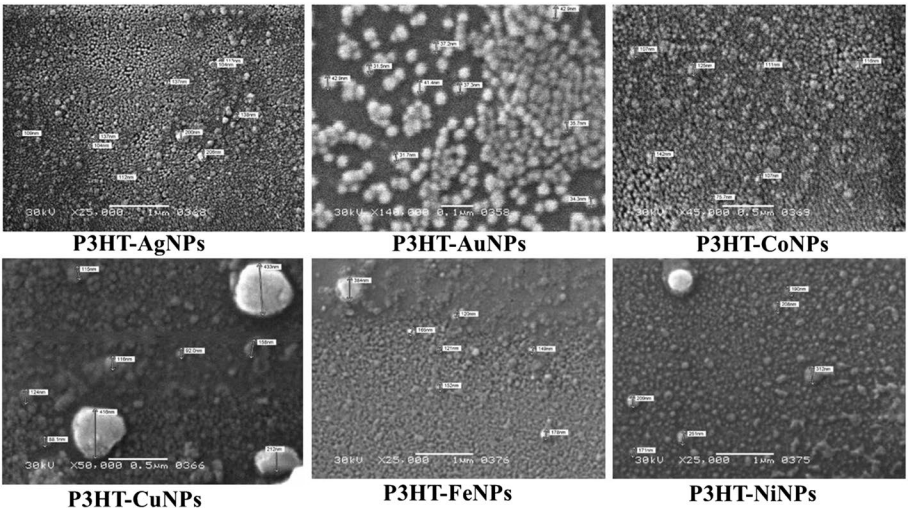

Fig. 2 SEM images of P3HT-MNPs

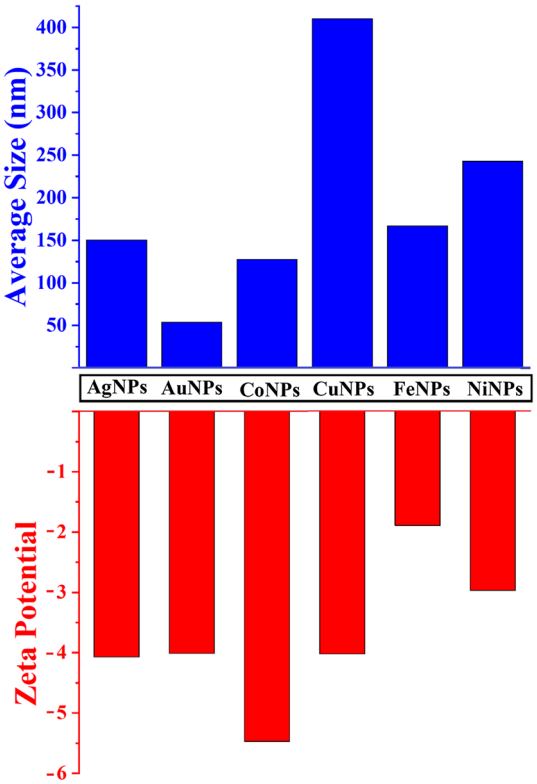

Fig. 3 Average size and zeta potential of P3HT-MNPs

population of particles having size less than 100 nm can also be noticed. In case of P3HT-CuNPs, there are many particles having size more than 400 nm while presence of another population having size around 100 nm is also evident. The size of P3HT-FeNPs is found be in a range of 120–180 nm. P3HT-NiNPs have particles mostly in the range of 170–250 nm while another population of particles having size around 100 nm is also evident.

The average particle sizes and apparent charges on the P3HT-MNPs were also determined by dynamic light scattering and zeta potential studies, Fig. 3. DLS results endorse the size ranges of MNPs as obtained by SEM for all six P3HT-MNPs under study. Furthermore, the zeta potential values in all cases were negative but not high which indicate their low long-term stability. Nonetheless, the intended application of the synthesized P3HT-MNPs is in the form of thin films.

The stabilization mechanism of Ag, Fe, Co, Ni, Au, and Cu nanoparticles with P3HT is investigated through FT-IR analysis, Fig. 4. This analysis is conducted for P3HT as well as for P3HT stabilized Ag, Fe, Co, Ni, Au, and Cu NPs. The peaks observed between 2900 and 3446 cm^{-1} correspond to the vibration of C–H bonds present in the aliphatic chain of the hexyl groups. The intensity of these peaks is notably high because the polymer contains a significant proportion of carbon–hydrogen bonds. However, the presence of a thiophene ring can be confirmed by the peak observed at 1454.6 cm^{-1}, while the peak at 1085 cm^{-1} confirms the existence of C–H bonds within the aromatic ring (Jin et al. 2014; Misra et al. 2014). The out-of-plane bending mode of the C–H group appeared at 816 cm^{-1}. The behavior of peaks in the range of 2900–3446 cm^{-1} of P3HT changed upon interaction with Ag, Fe, Co, Ni, Au, and Cu NPs. This behavior change is attributed to the interaction of the thiophene ring with the MNPs. Particularly, the peak at 1454.6 cm^{-1} in the P3HT spectrum changed its behavior in all P3HT stabilized MNPs spectra, indicating the interaction of the thiophene rings with the MNPs. Moreover, the peak at 1085 cm^{-1} of the aromatic ring has also changed its behavior for Ag, Fe, Co, Ni, Au, and Cu NPs which further confirmed the involvement of the thiophene ring in the stabilization of MNPs. The change in the core environment of the

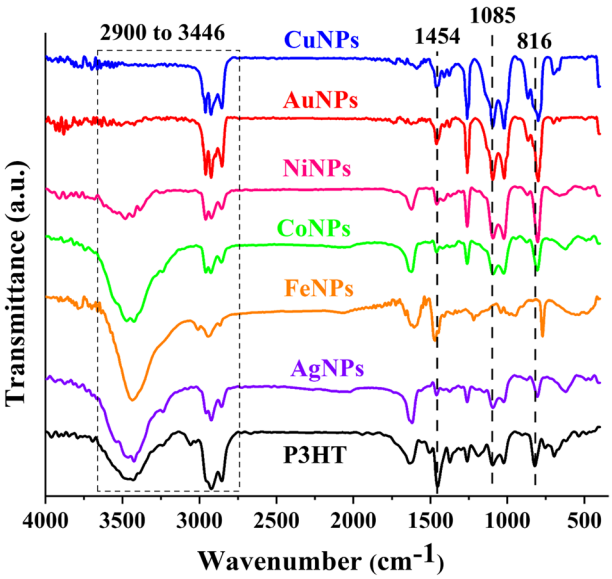

Fig. 4 FTIR spectra of P3HT and P3HT-MNPs

thiophene ring after interaction with MNPs also led to a slight right shift of the peak at 816 cm^{-1} of C–H bending (Guo et al. 2014; Rezaei et al. 2019; Usman et al. 2019).

3.2 Opto-electronic properties of P3HT-MNPs

The next step and actual target of this study is the evaluation of the impact of the incorporation of MNPs in P3HT on its optoelectronic properties in context of OSC (Lu et al. 2013). For this purpose, the optoelectronic properties of pristine polymer have to be determined in order to fairly evaluate the effect of the incorporation of MNPs. Optical bandgap of a semiconductor can be determined by Tauc plot or through of λ_{edge} of absorbance spectrum (Eom et al. 2017; Kesornsit et al. 2022). Herein, Optical bandgaps is determined by the method reported previously in which on-set wavelength or λ_{edge} of absorbance spectra is converted into eV (Acevedo-Peña et al. 2017; Ansari et al. 2022). The λ_{edge} of P3HT of UV–vis spectrum is found to be at 675 nm which translates into optical energy bandgap of 1.84 eV, Fig. 5A. This absorbance spectrum is quite similar in terms of shape with the absorbance spectrum observed by Acevedo-Peña et al. (Acevedo-Peña et al. 2017). However, slight change in on-set wavelength may be due to different molar mass or experimental conditions (Ansari et al. 2018; Ballantyne et al. 2008a). To determine the electrical bandgap of P3HT, on-set potentials have been evaluated from the cyclic voltammogram using reported method (Colladet et al. 2004; Ansari et al. 2018). The cyclic voltammogram of P3HT reveal the onset potential of oxidation at 1.03 V while onset potential of reduction at −0.91 V versus Ag/AgCl, Fig. 5B. Electrons are released as a result of oxidation from the π bonds of thiophene in P3HT that corresponds to HOMO level while electrons are added as a result of reduction that corresponds to the LUMO level. However, it is pertinent to mention here that obtained values are against Ag/AgCl which does not represent true HOMO and LUMO energy levels. The obtained values are however closely related to real HOMO and LUMO energy levels and are appropriate for comparison of different P3HT-MNPs. The optical energy bandgap for the pristine P3HT was found to be 1.94 eV. The shape of the cyclic voltammogram and onset potentials are similar to the previous reports (Kuila et al. 2010; Heeney et al. 2007; Lu et al. 2008). Slight changes in the onset potentials may be attributed to changes in molar mass, regioregularity, supporting electrolytes and experimental conditions.

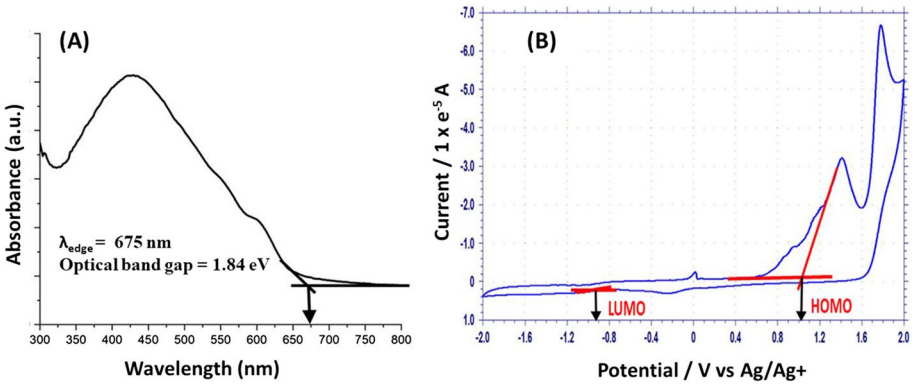

Fig. 5 Optoelectronic properties of parent P3HT film **A** UV–visible spectrophotometry, **B** Cyclic voltammetry

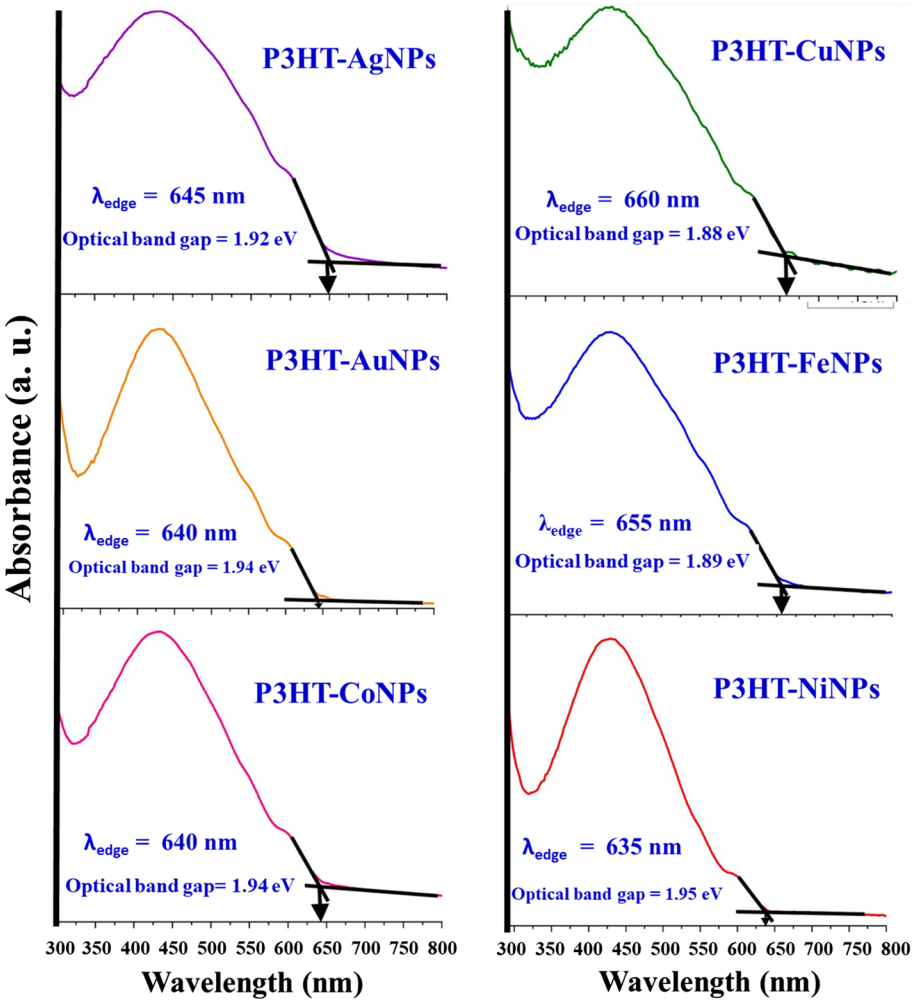

Fig. 6 UV–vis spectra of thin films of P3HT-MNPs

Conjugated polymer, P3HT, possess π electrons in the thiophene ring and a lone pair of electrons on sulfur, due to which this polymer may act as redox active polymer and a ligand for MNPs (Tanaka et al. 2017; Wang et al. 2018). Interaction of MNPs with P3HT can be considered in the same manner as in ligand–metal interaction (Sih and Wolf 2005; Grubbs 2007). UV–vis spectra of thin films of P3HT-MNPs are depicted in Fig. 6. We have noticed that absorption intensity has increased for some of the P3HT-MNPs, however, there is not a big shift in the absorption wavelength in all cases. The λ_{edge} of P3HT-AgNPs, P3HT-AuNPs, P3HT-CoNPs, P3HT-CuNPs, P3HT-FeNPs, and P3HT-NiNPs were found to be 645, 640, 640, 660, 655, and 635 nm, respectively. The optical energy band gap as calculated from λ_{edge} through Planck's quantum theory were 1.92, 1.94, 1.94, 1.88, 1.89, and 1.95 eV for P3HT-AgNPs, P3HT-AuNPs, P3HT-CoNPs, P3HT-CuNPs, P3HT-FeNPs, and P3HT-NiNPs in the same order. Slight variations in optical energy band gap might be attributed to the overlap of absorption spectra of P3HT and MNPs (Inagaki et al. 2018b).

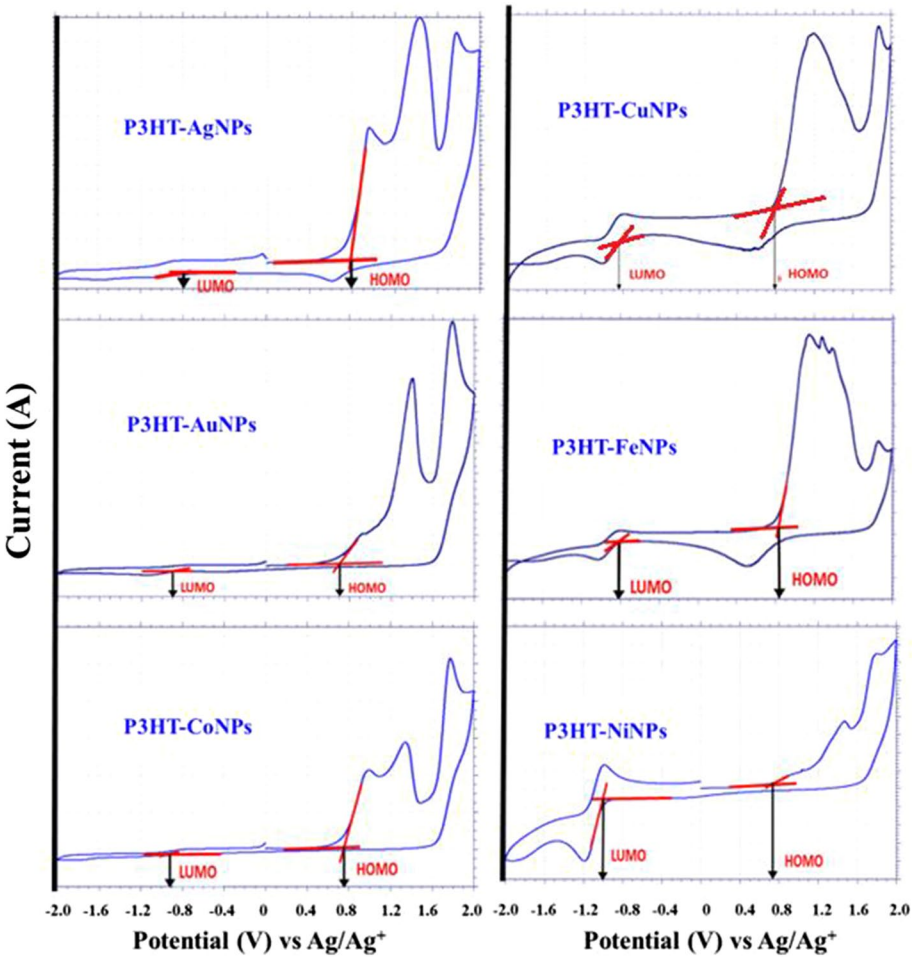

Fig. 7 Cyclic voltammogram of P3HT-MNPs

While incorporation of MNPs in P3HT did not induce any pronounced effect in the optical energy band gap despite an increase in the absorption intensity, the HOMO and LUMO energy levels have significantly shifted that induce a peculiar change in the electrical energy bad gap compared to pristine P3HT, see cyclic voltammograms in Fig. 7. It is well established fact that any electron donating or electron withdrawing functional group or metal may influence the HOMO, LUMO energy levels and subsequently the energy bandgap of the semiconductor (Hashemi et al. 2019; Long et al. 2017; Irfan et al. 2020). A comparison of optoelectronic properties of P3HT and P3HT-MNPs is presented in Fig. 8.

An electrochemical study of non-crystalline polythiophene/gold nanoparticles film showed oxidation peak of the film in a range of 0.6–0.9 V (vs. Ag/AgCl) for the different parts of chain of the polymer (Inagaki et al. 2018a). The onset oxidation potential for P3HT-AuNPs is observed at 0.71 (vs. Ag/AgCl) compared to 0.6 V (vs. Ag/AgCl) for polythiophene/AuNPs. The difference in the onset oxidation potential may be attributed to presence of hexyl group which may act as an electron donating group for the backbone of

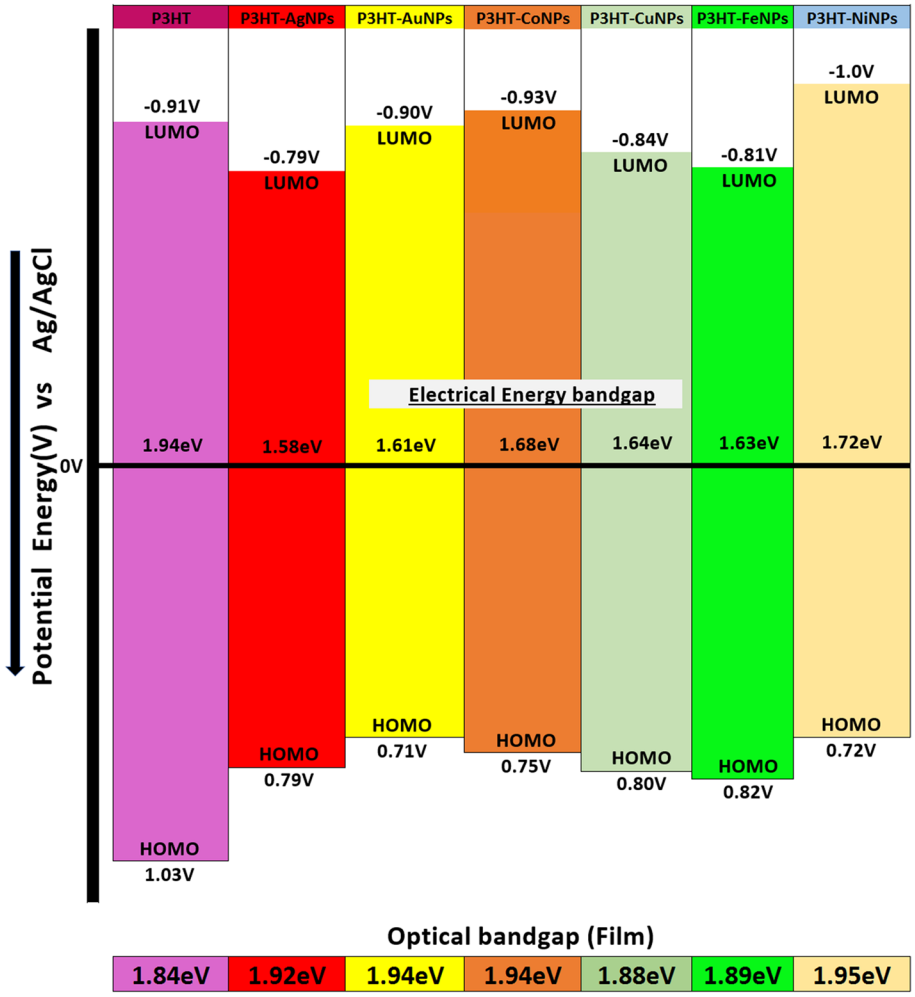

Fig. 8 Comparison of optoelectronic properties of P3HT-MNPs with pristine P3HT

conjugated polymer (P3HT). An upward shift of HOMO energy level for all P3HT-MNPs is noticed compared to parent P3HT. The electron accepting nature of metals induced an electron withdrawing effect on the conjugated system of P3HT that resulted in upshift of the HOMO level. The lowest upshift of HOMO level was observed for P3HT-FeNPs while highest for P3HT-AuNPs. This higher shift for gold compared to other metals may be attributed to its larger size and exceptional relevant properties such as relativistic effect. The electrons are bound to higher nuclear charge while electrons in d and f orbitals are least bound that render a resistance to oxidation. A clear trend of more upshifting with an increase in atomic size along a group (Cu, Ag, Au) can be noticed as also reported previously (Bartlett 1998). However, LUMO energy levels shift in both directions by incorporation of MNPs compared to parent P3HT. LUMO energy level is downshifted to −0.79 V for P3HT-AgNPs while upshifted to 1.0 V for P3HT-NiNPs from 0.91 V for P3HT.This different behavior may be attributed to the nature of the metal, its atomic size, and stability

of the electronic configuration. The effect of incorporation of transition metals (such as titanium, chromium, iron, and nickel) on HOMO–LUMO energy levels was significant that resulted in lowering of energy band gap (Lu et al. 2008).

Taking both the upshift of HOMO and downshift of LUMO into account reveal that electrical energy bandgap is compressed to highest extent for P3HT-AgNPs (1.58 eV) while lowest compression of electrical energy band gap is found for NiNPs-P3HT (1.72 eV). Hence, optoelectronic properties of P3HT-AgNPs are improved significantly compared to incorporation of other metals in P3HT. P3HT-AgNPs may be taken as the best composite material in context of OSC from the P3HT-MNPs explored in this study, as discussed in a recent review article (Meng et al. 2022).

Nonetheless, an appropriate alignment of energy levels of donor and acceptor materials is crucial for effective exciton mobility after light absorption. Incorporation of MNPs in P3HT donor material resulted in significant variations in the optoelectronic properties (such as energy levels and energy band gap). The strategy opens possibility of tailoring the energy levels and band gap as per energy levels of the acceptor material.

4 Conclusion

In the present study, incorporation of different MNPs based on Silver (Ag), Gold (Au), Cobalt (Co), Cupper (Cu), Iron (Fe), and Nickel (Ni) in P3HT is demonstrated. P3HT served as a good ligand for stabilization of these P3HT-MNPs. Size, shape, and morphology of P3HT-MNPs based on different metals vary significantly from each other. Although the wavelength of absorption of the solar spectrum is not affected to large extent by incorporation of different metallic ions in P3HT, electrical energy levels have significantly shifted. HOMO energy level is upshifted maximum for P3HT-AuNPs while LUMO energy level is maximum downshifted for P3HT-AgNPs. Overall, maximum electrical energy band gap reduction is achieved for P3HT-AgNPs. The study reveals the method for better alignment of energy levels of donor for any acceptor by incorporation of metals in donor materials (P3HT in this case).

Author contributions All authors contributed to the study conception and design. Material preparation, data collection and analysis were performed by SR, MAA, DAR, HT, and MM. The first draft of the manuscript was written by SR and MAA, and all authors commented on previous versions of the manuscript. All authors read and approved the final manuscript.

Funding Financial support by Pakistan Science Foundation under scheme Pak-Sri Lanka Joint Projects (Project No. PSF-NSF/Eng/S-HEJ 03) is gratefully acknowledged.

Data availability The datasets generated during and/or analyzed during the current study are available from the corresponding author on reasonable request.

Declarations

Conflict of interest Authors declare no conflict of interest.

Ethical approval Not Applicable.

References

Abdullah, E.T., Ibrahim, O.A.: 'Capacitance and resistivity measurements of polythiophene /metallic nanoparticles-based humidity sensors. Iraqi J. Sci. **62**, 1158–1163 (2021)

Acevedo-Peña, P., Baray-Calderón, A., Hailin, Hu., González, I., Ugalde-Saldivar, V.M.: Measurements of HOMO-LUMO levels of poly(3-hexylthiophene) thin films by a simple electrochemical method. J. Solid State Electrochem. **21**, 2407–2414 (2017)

Ameri, T., Khoram, P., Min, J., Brabec, C.J.: Organic ternary solar cells: a review. Adv. Mater. **25**, 4245–4266 (2013)

Ansari, M.A., Mohiuddin, S., Kandemirli, F., Malik, M.I.: Synthesis and characterization of poly(3-hexylthiophene): improvement of regioregularity and energy band gap. RSC Adv. **8**, 8319–8328 (2018)

Ansari, M.A., Hafeez, A., Mustafa, M., Wijesundera, R.P., Malik, M.I.: Molecular tailoring of donor and acceptor materials of organic solar cells for improvement of their optoelectronic properties. Mater. Sci. Semicond. Process. **150**, 106919 (2022)

Ballantyne, A.M., Chen, L., Dane, J., Hammant, T., Braun, F.M., Heeney, M., Duffy, W., McCulloch, I., Bradley, D.D.C., Nelson, J.: The effect of poly (3-hexylthiophene) molecular weight on charge transport and the performance of polymer: fullerene solar cells. Adv. Funct. Mater. **18**, 2373–2380 (2008a)

Ballantyne, A.M., Chen, L., Dane, J., Hammant, T., Braun, F.M., Heeney, M., Duffy, W., McCulloch, I., Bradley, D.D.C., Nelson, J.: The effect of poly(3-hexylthiophene) molecular weight on charge transport and the performance of polymer: fullerene solar cells. Adv. Funct. Mater. **18**, 2373–2380 (2008b)

Bartlett, N.: Relativistic effects and the chemistry of gold. Gold Bull. **31**, 22–25 (1998)

Blakesley, J.C., Neher, D.: Relationship between energetic disorder and open-circuit voltage in bulk heterojunction organic solar cells. Phys. Rev. B **84**, 075210 (2011)

Boriskina, S.V., Ghasemi, H., Chen, G.: Plasmonic materials for energy: from physics to applications. Mater. Today **16**, 375–386 (2013)

Brédas, J.L., Heeger, A.J.: Influence of donor and acceptor substituents on the electronic characteristics of poly(paraphenylene vinylene) and poly(paraphenylene). Chem. Phys. Lett. **217**, 507–512 (1994)

Chen, T.-A., Xiaoming, Wu., Rieke, R.D.: Regiocontrolled synthesis of poly (3-alkylthiophenes) mediated by Rieke zinc: their characterization and solid-state properties. J. Am. Chem. Soc. **117**, 233–244 (1995)

Cheng, Y.-J., Yang, S.-H., Hsu, C.-S.: Synthesis of conjugated polymers for organic solar cell applications. Chem. Rev. **109**, 5868–5923 (2009)

Chen, Z., Chen, B., He, M., Wang, H., Bin, Hu.: A porous organic polymer with magnetic nanoparticles on a chip array for preconcentration of platinum(IV), gold(III) and bismuth(III) prior to their on-line quantitation by ICP-MS. Microchim. Acta **186**, 107 (2019)

Colladet, K., Nicolas, M., Goris, L., Lutsen, L., Vanderzande, D.: Low-band gap polymers for photovoltaic applications. Thin Solid Films **451–452**, 7–11 (2004)

de Freitas, J.N., Mamo, M.A., Maubane, M., van Otterlo, W.A.L., Coville, N.J., Nogueira, A.F.: Nanocomposites of gold and poly(3-hexylthiophene) containing fullerene moieties: synthesis, characterization and application in solar cells. J. Power Sources **215**, 99–108 (2012)

Eakins, G.L., Alford, J.S., Tiegs, B.J., Breyfogle, B.E., Stearman, C.J.: Tuning HOMO–LUMO levels: trends leading to the design of 9-fluorenone scaffolds with predictable electronic and optoelectronic properties. J. Phys. Org. Chem. **24**, 1119–1128 (2011)

Eom, K., Kwon, U., Kalanur, S.S., Park, H.J., Seo, H.: Depth-resolved band alignments of perovskite solar cells with significant interfacial effects. J. Mater. Chem. A **5**, 2563–2571 (2017)

Franco, I.B., Power, C., Whereat, J.: SDG 7 affordable and clean energy. In: Franco, I.B., Chatterji, T., Derbyshire, E., Tracey, J. (eds.) Actioning the global goals for local impact. Springer, Berlin (2020)

Gan, Q., Bartoli, F.J., Kafafi, Z.H.: Plasmonic-enhanced organic photovoltaics: breaking the 10% efficiency barrier. Adv. Mater. **25**, 2385–2396 (2013)

Gao, Y., Liu, M., Zhang, Y., Liu, Z., Yang, Y., Zhao, L.: Recent development on narrow bandgap conjugated polymers for polymer solar cells. Polymers **9**, 39 (2017)

Grubbs, R.B.: Roles of polymer ligands in nanoparticle stabilization. Polym. Rev. **47**, 197–215 (2007)

Guo, Q., Zou, S., Li, J., Li, D., Jiao, H., Shi, J.: Facile synthesis of morphology- and size-controllable polythiophene/gold composites in aqueous medium. J. Nanopart Res. **16**, 2702 (2014)

Hashemi, D., Ma, X., Ansari, R., Kim, J., Kieffer, J.: Design principles for the energy level tuning in donor/acceptor conjugated polymers. Phys. Chem. Chem. Phys. **21**, 789–799 (2019)

Heeney, M., Zhang, W., Crouch, D.J., Chabinyc, M.L., Gordeyev, S., Hamilton, R., Higgins, S.J., McCulloch, I., Skabara, P.J., Sparrowe, D., Tierney, S.: Regioregular poly (3-hexyl) selenophene: a low band gap organic hole transporting polymer. Chem. Commun. **47**, 5061–5063 (2007)

Hoppe, H., Sariciftci, N.S.: Organic solar cells: an overview. J. Mater. Res. **19**, 1924–1945 (2004)

Huang, Ye., Guo, X., Liu, F., Huo, L., Chen, Y., Russell, T.P., Han, C.C., Li, Y., Hou, J.: Improving the ordering and photovoltaic properties by extending π–conjugated area of electron-donating units in polymers with D-A structure. Adv. Mater. **24**, 3383–3389 (2012)

Inagaki, C.S., Oliveira, M.M., Zarbin, A.J.G.: Direct and one-step synthesis of polythiophene/gold nanoparticles thin films through liquid/liquid interfacial polymerization. J Colloid Interface Sci **516**, 498–510 (2018a)

Inagaki, C.S., Oliveira, M.M., Zarbin, A.J.G.: Direct and one-step synthesis of polythiophene/gold nanoparticles thin films through liquid/liquid interfacial polymerization. J. Colloid Interface Sci. **516**, 498–510 (2018b)

Irfan, A., Al-Sehemi, A.G., Assiri, M.A., Ullah, S.: Exploration the effect of metal and electron withdrawing groups on charge transport and optoelectronic nature of schiff base Ni(II), Cu(II) and Zn(II) complexes at molecular and solid-state bulk scales. Mater. Sci. Semicond. Process. **107**, 104855 (2020)

Jana, B., Bhattacharyya, S., Patra, A.: Conjugated polymer P3HT–Au hybrid nanostructures for enhancing photocatalytic activity. Phys. Chem. Chem. Phys. **17**, 15392–15399 (2015)

Jenkins, J.L., Lee, P.A., Nebesny, K.W., Ratcliff, E.L.: Systematic electrochemical oxidative doping of P3HT to probe interfacial charge transfer across polymer–fullerene interfaces. J. Mater. Chem. A **2**, 19221–19231 (2014)

Jin, H.-D., Zheng, F., Xu, W.-L., Yuan, W.-H., Zhu, M.-Q., Hao, X.-T.: The structure and optical properties of regio-regular poly(3-hexylthiophene) and carboxylic multi-walled carbon nanotubes composite films. J. Phys. d Appl. Phys. **47**, 505502 (2014)

Kaçuş, H., Biber, M., Aydoğan, Ş: Role of the Au and Ag nanoparticles on organic solar cells based on P3HT:PCBM active layer. Appl. Phys. A **126**, 817 (2020)

Kango, S., Kalia, S., Celli, A., Njuguna, J., Habibi, Y., Kumar, R.: Surface modification of inorganic nanoparticles for development of organic–inorganic nanocomposites—a review. Prog. Polym. Sci. **38**, 1232–1261 (2013)

Kesornsit, S., Direksilp, C., Phasuksom, K., Thummarungsan, N., Sakunpongpitiporn, P., Rotjanasuworapong, K., Sirivat, A., Niamlang, S.: Synthesis of highly conductive poly(3-hexylthiophene) by chemical oxidative polymerization using surfactant templates. Polymers **14**, 3860 (2022)

Kravets, V.G., Kabashin, A.V., Barnes, W.L., Grigorenko, A.N.: Plasmonic surface lattice resonances: a review of properties and applications. Chem. Rev. **118**, 5912–5951 (2018)

Kroon, R., Lenes, M., Hummelen, J.C., Blom, P.W.M., de Boer, B.: Small bandgap polymers for organic solar cells (polymer material development in the last 5 years). Polym. Rev. **48**, 531–582 (2008)

Kuila, B.K., Garai, A., Nandi, A.K.: Synthesis, optical, and electrical characterization of organically soluble silver nanoparticles and their poly(3-hexylthiophene) nanocomposites: enhanced luminescence property in the nanocomposite thin films. Chem. Mater. **19**, 5443–5452 (2007)

Kuila, B.K., Park, K., Dai, L.: Soluble P3HT-grafted carbon nanotubes: synthesis and photovoltaic application. Macromolecules **43**, 6699–6705 (2010)

Leclerc, N., Michaud, A., Sirois, K., Morin, J.-F., Leclerc, M.: Synthesis of 2,7-carbazolenevinylene-based copolymers and characterization of their photovoltaic properties. Adv. Funct. Mater. **16**, 1694–1704 (2006)

Li, G., Shrotriya, V., Yao, Y., Huang, J., Yang, Y.: Manipulating regioregular poly(3-hexylthiophene): [6,6]-phenyl-C61-butyric acid methyl ester blends—route towards high efficiency polymer solar cells. J. Mater. Chem. **17**, 3126–3140 (2007)

Li, Y., Huang, W., Dejiang Zhao, Lu., Wang, Z.J., Huang, Q., Wang, P., Sun, M., Yuan, G.: Recent progress in organic solar cells: a review on materials from acceptor to donor. Molecules **27**, 1800 (2022)

Liu, C., Wang, K., Gong, X., Heeger, A.J.: Low bandgap semiconducting polymers for polymeric photovoltaics. Chem. Soc. Rev. **45**, 4825–4846 (2016)

Long, X., Dou, C., Liu, J., Wang, L.: Fine-tuning LUMO energy levels of conjugated polymers containing a B←N Unit. Macromolecules **50**, 8521–8528 (2017)

Lu, J., Liang, F., Drolet, N., Ding, J., Tao, Y., Movileanu, R.: Crystalline low band-gap alternating indolocarbazole and benzothiadiazole-cored oligothiophene copolymer for organic solar cell applications. Chem. Commun. **42**, 5315–5317 (2008)

Lu, L., Luo, Z., Tao, Xu., Luping, Yu.: cooperative plasmonic effect of Ag and au nanoparticles on enhancing performance of polymer solar cells. Nano Lett. **13**, 59–64 (2013)

Ludwigs, S.: P3HT revisited—from molecular scale to solar cell devices. Springer, Berlin, Heidelberg (2014)

Mathews, I., Kantareddy, S.N., Buonassisi, T., Peters, I.M.: Technology and market perspective for indoor photovoltaic cells. Joule **3**, 1415–1426 (2019)

Mbuyise, X.G., Dlamini, M.W., Mola, G.T.: Metal nano-composite induced light trapping and enhanced solar cell performances. Phys. b Condens. Matter **622**, 413321 (2021)

Meng, D., Zheng, R., Zhao, Y., Zhang, E., Dou, L., Yang, Y.: Near-infrared materials: the turning point of organic photovoltaics. Adv. Mater. **34**, 2107330 (2022)
Misra, R.D.K., Depan, D., Challa, V.S.A., Shah, J.S.: Supramolecular structures fabricated through the epitaxial growth of semiconducting poly(3-hexylthiophene) on carbon nanotubes as building blocks of nanoscale electronics. Phys. Chem. Chem. Phys. **16**, 19122–19129 (2014)
Monnaie, F., Brullot, W., Verbiest, T., De Winter, J., Gerbaux, P., Smeets, A., Koeckelberghs, G.: Synthesis of end-group functionalized P3HT: general protocol for P3HT/nanoparticle hybrids. Macromolecules **46**, 8500–8508 (2013)
Nicholson, P.G., Ruiz, V., Macpherson, J.V., Unwin, P.R.: Enhanced visible photoluminescence in ultrathin poly(3-hexylthiophene) films by incorporation of Au nanoparticles. Chem. Commun. **8**, 1052–54 (2005)
Padinger, F., Rittberger, R.S., Sariciftci, N.S.: Effects of postproduction treatment on plastic solar cells. Adv. Funct. Mater. **13**, 85–88 (2003)
Peet, J., Kim, J.Y., Coates, N.E., Ma, W.L., Moses, D., Heeger, A.J., Bazan, G.C.: Efficiency enhancement in low-bandgap polymer solar cells by processing with alkane dithiols. Nat. Mater. **6**, 497–500 (2007)
Perepichka, D.F., Bryce, M.R.: Molecules with exceptionally small HOMO–LUMO gaps. Angew. Chem. Int. Ed. **44**, 5370–5373 (2005)
Ratcliff, E.L., Lee, P.A., Armstrong, N.R.: Work function control of hole-selective polymer/ITO anode contacts: an electrochemical doping study. J. Mater. Chem. **20**, 2672–2679 (2010)
Rezaei, B., Afshar-Taromi, F., Ahmadi, Z., Rigi, S.A., Yousefi, N.: Enhancement of power conversion efficiency of bulk heterojunction polymer solar cells using core/shell, Au/graphene plasmonic nanostructure. Mater. Chem. Phys. **228**, 325–335 (2019)
Sachchidan, Samajdar, D.P.: Light-trapping strategy for PEDOT:PSS/c-Si nanopyramid based hybrid solar cells embedded with metallic nanoparticles. Sol. Energy **190**, 278–85 (2019)
Saeki, A., Ohsaki, S.-I., Seki, S., Tagawa, S.: Electrodeless determination of charge carrier mobility in poly(3-hexylthiophene) films incorporating perylenediimide as photoconductivity sensitizer and spectroscopic probe. J. Phys. Chem. C **112**, 16643–16650 (2008)
Schilinsky, P., Asawapirom, U., Scherf, U., Biele, M., Brabec, C.J.: Influence of the molecular weight of poly(3-hexylthiophene) on the performance of bulk heterojunction solar cells. Chem. Mater. **17**, 2175–2180 (2005)
Shnoudeh, A.J., Hamad, I., Abdo, R.W., Qadumii, L., Jaber, A.Y., Surchi, H.S., Alkelany, S.Z.: Chapter 15 - Synthesis, characterization, and applications of metal nanoparticles. In: Tekade, Rakesh K. (ed.) Biomaterials and bionanotechnology. Academic Press, Cambridge (2019)
Sih, B.C., Wolf, M.O.: Metal nanoparticle—conjugated polymer nanocomposites. Chem. Commun. **27**, 3375–84 (2005)
Skompska, M., Szkurłat, A.: The influence of the structural defects and microscopic aggregation of poly(3-alkylthiophenes) on electrochemical and optical properties of the polymer films: discussion of an origin of redox peaks in the cyclic voltammograms. Electrochim. Acta **46**, 4007–4015 (2001)
Stuart, H.R., Hall, D.G.: Island size effects in nanoparticle-enhanced photodetectors. Appl. Phys. Lett. **73**, 3815–3817 (1998)
Sun, C., Pan, F., Bin, H., Zhang, J., Xue, L., Qiu, B., Wei, Z., Zhang, Z.-G., Li, Y.: A low cost and high performance polymer donor material for polymer solar cells. Nat. Commun. **9**, 743 (2018)
Szeremeta, J., Nyk, M., Chyla, A., Strek, W., Samoc, M.: Enhancement of photoconduction in a conjugated polymer through doping with copper nanoparticles. Opt. Mater. **33**, 1372–1376 (2011)
Tanaka, S., Rosli, S.K.B., Takada, K., Taniai, N., Yoshitomi, T., Ando, H., Matsumoto, K.: Effects of bromination of poly(3-hexylthiophene) on the performance of bulk heterojunction solar cells. RSC Adv. **7**, 46874–46880 (2017)
Topp, K., Borchert, H., Johnen, F., Tunc, A.V., Knipper, M., von Hauff, E., Parisi, J., Al-Shamery, K.: Impact of the Incorporation of Au Nanoparticles into Polymer/Fullerene Solar Cells. J. Phys. Chem. A **114**, 3981–3989 (2010)
Trznadel, M., Pron, A., Zagorska, M., Chrzaszcz, R., Pielichowski, J.: Effect of molecular weight on spectroscopic and spectroelectrochemical properties of regioregular poly(3-hexylthiophene). Macromolecules **31**, 5051–5058 (1998)
Usman, K., Al-Ghouti, M.A., Abu-Dieyeh, M.H.: The assessment of cadmium, chromium, copper, and nickel tolerance and bioaccumulation by shrub plant Tetraena qataranse. Sci. Rep. **9**, 5658 (2019)
Wang, X., Zheng, Y., Lan, Xu.: An electrochemical adenine sensor employing enhanced three-dimensional conductivity and molecularly imprinted sites of Au NPs bridged poly(3-thiophene acetic acid). Sens. Actuators B Chem. **255**, 2952–2958 (2018)
Warren, S.C., Thimsen, E.: Plasmonic solar water splitting. Energy Environ. Sci **5**, 5133–5146 (2012)

Xin, H., Kim, F.S., Jenekhe, S.A.: Highly efficient solar cells based on poly(3-butylthiophene) nanowires. J. Am. Chem. Soc. **130**, 5424–5425 (2008)
Xin, H., Reid, O.G., Ren, G., Kim, F.S., Ginger, D.S., Jenekhe, S.A.: Polymer nanowire/fullerene bulk heterojunction solar cells: how nanostructure determines photovoltaic properties. ACS Nano **4**, 1861–1872 (2010)
Xu, X., Li, D., Yuan, J., Zhou, Y., Zou, Y.: Recent advances in stability of organic solar cells. EnergyChem **3**, 100046 (2021)
Yang, Y.: The original design principles of the Y-series nonfullerene acceptors, from Y1 to Y6. ACS Nano **15**, 18679–18682 (2021)
Yao, K., Zhong, H., Liu, Z., Xiong, M., Leng, S., Zhang, J., Yun-xiang, Xu., Wang, W., Zhou, L., Huang, H., Jen, A.K.Y.: Plasmonic metal nanoparticles with core-bishell structure for high-performance organic and perovskite solar cells. ACS Nano **13**, 5397–5409 (2019)
Zhang, M., Guo, X., Yang, Y., Zhang, J., Zhang, Z.-G., Li, Y.: Downwards tuning the HOMO level of polythiophene by carboxylate substitution for high open-circuit-voltage polymer solar cells. Polym. Chem. **2**, 2900–2906 (2011)
Zhang, Y., Lim, C.-K., Dai, Z., Guannan, Yu., Haus, J.W., Zhang, H., Prasad, P.N.: Photonics and optoelectronics using nano-structured hybrid perovskite media and their optical cavities. Phys. Rep. **795**, 1–51 (2019)
Zhang, X., Yao, C., Zhao, J., Ali, M.U., Li, A., Shen, C.-F., Yan, C., He, Y., Miao, J., Meng, H.: Molecular tailoring of trifluoromethyl-substituted conjugated polymers for efficient organic solar cells. Polym. Chem. **12**, 3346–3351 (2021)
Zhao, W., Li, S., Yao, H., Zhang, S., Zhang, Y., Yang, B., Hou, J.: Molecular optimization enables over 13% efficiency in organic solar cells. J. Am. Chem. Soc. **139**, 7148–7151 (2017)
Zhou, H., Yang, L., Stuart, A.C., Price, S.C., Liu, S., You, W.: Development of fluorinated benzothiadiazole as a structural unit for a polymer solar cell of 7% efficiency. Angew. Chem. **123**, 3051–3054 (2011)
Zhou, Na., López-Puente, V., Wang, Q., Polavarapu, L., Pastoriza-Santos, I., Qing-Hua, Xu.: Plasmon-enhanced light harvesting: applications in enhanced photocatalysis, photodynamic therapy and photovoltaics. RSC Adv. **5**, 29076–29097 (2015)
Zhu, L., Zhang, M., Jinqiu, Xu., Li, C., Yan, J., Zhou, G., Zhong, W., Hao, T., Song, J., Xue, X., Zhou, Z., Zeng, R., Zhu, H., Chen, C.-C., MacKenzie, R.C.I., Zou, Y., Nelson, J., Zhang, Y., Sun, Y., Liu, F.: Single-junction organic solar cells with over 19% efficiency enabled by a refined double-fibril network morphology. Nat. Mater. **21**, 656–663 (2022)